Journal of Drug Delivery Science and Technology 101 (2024) 106214

Contents lists available at ScienceDirect

Journal of Drug Delivery Science and Technology

journal homepage: www.elsevier.com/locate/jddst

AT11-guided liposomes for oral cancer cells: From characterization towards *in vitro* evaluation

Jéssica Lopes-Nunes [a], Maria Paula Cabral Campello [b,c], António Paulo [b,c], Claudio Nastruzzi [d], Paula A. Oliveira [e,g], Carla Cruz [a,f,*]

[a] CICS-UBI - Health Sciences Research Centre, University of Beira Interior, Covilhã, Portugal
[b] Centro de Ciências e Tecnologias Nucleares, Instituto Superior Técnico, Universidade de Lisboa, Estrada Nacional 10 (km 139.7), 2695-066, Bobadela, Portugal
[c] Departamento de Engenharia e Ciências Nucleares, Instituto Superior Técnico, Universidade de Lisboa, Estrada Nacional 10 (km 139.7), 2695-066, Bobadela, Portugal
[d] Department of Chemical, Pharmaceutical and Agricultural Sciences, University of Ferrara, Ferrara, Italy
[e] Centre for the Research and Technology of Agro-Environmental and Biological Sciences (CITAB), University of Trás-os-Montes and Alto Douro (UTAD), Vila Real, Portugal
[f] Departamento de Química, Universidade da Beira Interior, Rua Marquês de Ávila e Bolama, 6201-001, Covilhã, Portugal
[g] Inov4Agro, Institute for Innovation, Capacity Building and Sustainability of Agri-food Production, Vila Real, Portugal

ARTICLE INFO

Keywords:
Oral cancer
Acridine orange derivative
Aptamer
Liposomes

ABSTRACT

The increasing prevalence of oral cancers, particularly those attributed to human papillomavirus infection, along with the associated drawbacks of conventional therapies, has spurred research into more effective treatment modalities. Liposomes have emerged as a potential strategy to improve the delivery of anticancer molecules to the cells of interest. However, functionalizing these nanoparticles with targeting agents could significantly enhance their selectivity. A prospective approach involves the incorporation of aptamers, which facilitate drug accumulation within cancer cells. Among these, the AT11 aptamer has garnered attention due to its improved toxicity and high affinity to nucleolin, making it a promising targeting moiety. Therefore, we propose to use AT11 for liposomes' functionalization, to enhance the selectivity of C_8, a potential anticancer compound, specifically targeting oral cancer cells. Thus, we produced liposomes (empty or C_8-associated) by ethanol injection method and, then, proceeded with their functionalization with AT11-TEG-Cholesteryl. The resulting liposomes were characterized by dynamic light scattering and hydrodynamic diameters of 130–136 nm were obtained. Additionally, the effect of the produced liposomes on the viability of squamous cell carcinoma of the tongue (UPCI-SCC-154) and nonmalignant (Het1A) cells was determined, by MTT assay. It was demonstrated that the viability of cells treated with empty liposomes was almost unaffected until the 53.6 μg/mL concentration. After treating the cells with C_8-associated liposomes, both cell lines showed a dose-response effect. Moreover, the AT11-functionalization of the obtained C_8-associated liposomes enhanced the selectivity of the liposomes towards oral cancer cell line, as observed by the MTT assay (43.2 % in UPCI-SCC-154 versus 79.4 % in Het1A) and confocal microscopy. Furthermore, the anticancer potential of AT11 C_8-associated liposomes was evaluated in terms of proliferation (ki67 positive cells), cell death (propidium iodide internalization in non-permeabilized cells and caspase-3 activity), migration (cell scratch assay) and invasion. Overall, the produced liposomes decreased tongue cancer cell proliferation (53.6 % versus 99.4 %), migration (from 24.6 % to −3.8 %) and invasion (to 19 %) and induced cell death (11.6-fold increase in propidium iodide positive cells, and a 140 % of caspase-3 activity). These findings suggest that the AT11 C_8-associated liposomes are promising drug carriers for oral cancer therapy.

1. Introduction

Oral cancer is a common and aggressive cancer with a poor prognosis, affecting oral epithelial cells in regions such as the floor of the mouth, alveolar and the hard palate, with the tongue being the most frequently affected subsite [1,2]. Moreover, patients may develop

* Corresponding author. CICS-UBI - Health Sciences Research Centre, University of Beira Interior, Covilhã, Portugal.
E-mail address: carlacruz@fcsaude.ubi.pt (C. Cruz).

https://doi.org/10.1016/j.jddst.2024.106214
Received 22 April 2024; Received in revised form 14 September 2024; Accepted 17 September 2024
Available online 19 September 2024

metastasis, leading to a high mortality rate [3]. Its carcinogenesis is typically linked to genetic mutations, often associated with long-term exposure to risk factors such as smoking or alcohol consumption [3]. Additionally, human papillomavirus (HPV) infection, especially HPV16 which is the most commonly detected, plays an important role in the initiation and progression of oral cancer [4,5]. In this case, the oncogenesis results essentially from the HPV oncoproteins E6 and E7 that, among other functions, degrade and inactivate the tumor suppressor proteins p53 and pRB, respectively [6]. Over the years, HPV-related oral cancer incidence rates have been increasing, especially in men [1]. For these patients, the conventional therapies consist mainly in surgery, chemo and radiotherapy alone or in combination. These treatment options have made important progress, but they are associated with several adverse side effects that can result in permanent healthy tissue damage [7]. Additionally, oral cancer is often diagnosed in an advanced and untreatable stage in which the cells have become aggressive and resistant to therapeutic drugs [8].

To address the challenges associated with conventional anticancer drugs, nanomedicines are emerging as more effective therapeutic approaches, capable of increasing drug bioavailability with optimized biodistribution to enhance the selective uptake by the tumoral cells [7]. In this area, liposomes are being widely tested and already employed for treating certain cancers, demonstrating to be good candidates for the delivery of chemotherapeutic drugs to the tumor. Some initial results suggest that this type of nanoparticles represents a suitable option for the treatment of oral cancer, namely for gene delivery [9], drug delivery [10–13] and photodynamic therapy [14]. Additionally, the use of targeted drug delivery systems, obtained by functionalizing nanoparticles with aptamers, designed for oral cancer treatment, can reduce systemic toxicity [7].

Aptamers are single-stranded oligonucleotides with high affinity to a certain target (e.g. proteins, small molecules, ions, or even whole cells) [15]. For instance, G-quadruplex (G4) aptamers have a higher negative charge density compared to duplex DNA, which favors their interaction with positively charged proteins or small molecules [16]. These molecules proved to be promising targeting moieties since they can discriminate between oncogenic and non-oncogenic forms of proteins [15]. A widely known G4 aptamer is the AS1411, which has a high affinity towards nucleolin, a protein overexpressed on several cancer cells' surfaces [17–20]. AS1411 was tested in clinical trials but demonstrated low potency and suboptimal pharmacology [21]. More recently, this aptamer has been used as a targeting agent for the specific delivery of small molecules and different types of nanoparticles [15]. To achieve better structural or antiproliferative results, derivatives of AS1411 are being proposed. For instance, AT11 is an oligonucleotide derived from AS1411 by adding thymine nucleotides to both 5′- and 3′-ends of the DNA sequence and a single G-to-T modification at position 11, forming a single major G4 conformation that enhances its anti-proliferative effects [22,23]. In this context, we designed liposomes coupled with the AT11, to deliver the acridine orange derivative (10-(8-(4-iodobenzamide) octyl)-3,6-bis (dimethylamine) acridinium iodide, C_8) more selectivity towards HPV-related oral cancer cells. This acridine is a G4-ligand presents a potential dual antiviral [24] and anticancer effect, as previously reported by our group [18,23,25,26]. Although its specific action mechanism is still unknown and it has been associated with a high affinity for binding to ($K_D \sim 10^{-7}$ M) and stabilizing G-rich sequences into G4 secondary structures [18,26]. These G-rich sequences are found in regulatory regions such as gene promoters (including oncogenes, e.g. KRAS or c-Myc), telomere ends, 5′-unstranslated regions of mRNAs, and viral genomes, such as high-risk HPVs [16,24]. Its therapeutic effect was putatively attributed to its ability to induce G4 stabilization in G-rich sequences thus disrupting the regulation of several key processes, including telomere elongation and maintenance, DNA replication, transcription, and translation [25,26]. Consequently, this compound may be a promising therapeutic approach in cancers arising from persistent HPV infection, such as certain oral cancers. However, like other anticancer drugs, it lacks selectivity for cancer cells and can also be cytotoxic to nonmalignant cells [26].

In light of the above-mentioned, this paper describes the use of C_8-associated liposomes functionalized with AT11 for treating HPV-related oral cancer cells. First, the production and characterization of liposomes loaded with C_8 and functionalized with AT11 aptamer were examined. Subsequently, *in vitro* biological effects were assessed, for instance, cell viability and internalization tests were carried out using the MTT assay and confocal microscopy, respectively. Finally, the effects of the liposomes on cancer proliferation, apoptosis, migration, and invasion were also assessed.

2. Materials and methods

2.1. Materials

Cholesterol (CAS: 57-88-5) was acquired from Sigma-Aldrich, palmitic acid (CAS: 57-10-3) from BHD Laboratory Reagents, and soybean phosphatidylcholine (PHOSPHOLIPON® 90G) was generously donated by Lipoid Kosmetik™. The lipid solutions consisted of 130 mg/mL phosphatidylcholine (171.5 mM) and 12.5 mg/mL cholesterol (32.3 mM) dissolved in 99.5 % ethanol.

The AT11 aptamer (5′-TGG-TGG-TGG-TTG-TTG-TGG-TGG-TGG-TGG-T-Cholesteryl-TEG-3′) and Cy5-labelled AT11 were purchased from Eurogentec (Belgium), and the stock solution was prepared with 100 μL of Milli-Q water and stored at −20 °C until needed. The concentration of the oligonucleotide was determined via spectrophotometry by measuring the absorbance at 260 nm with a UV–Vis spectrophotometer (Thermo Scientific™ Evolution 220) using the molar extinction coefficient (ε) provided.

Synthesis and purification of the ligand C_8 (10-(8-(4-iodobenzamide) octyl))-3,6-bis(dimethylamine) acridinium iodide was performed as previously described [27] and a 1 mM stock solution was prepared in 99.5 % ethanol.

Nonmalignant epithelial cells isolated from the esophagus (Het1A; ref. CRL-2692™) were obtained from ATCC and carcinoma of the tongue (UPCI-SCC-154; ref. ACC669) cells were obtained from DSMZ. DMEM (Dulbecco's Modified Eagle Medium) was purchased from Corning Life Sciences (AZ, USA). MEM (Minimal Essential Medium) was purchased from Gibco, Thermo Scientific™ (MA, USA), and MEM Non-Essential Amino Acid Solution (100×) from Sigma Aldrich (MO, USA).

Hoechst 33342, 3-[4,5-dimethylthiazol-2-yl]-2,5 diphenyl tetrazolium bromide (MTT) (CAS: 298-93-1) and Dimethyl sulfoxide (DMSO) (CAS: 67-68-5) were acquired from Thermo Fisher Scientific™ (Waltham, MA, USA).

2.2. Methods

2.2.1. Liposomes production

Liposomes were prepared using the ethanol injection method. The lipid solution was prepared by mixing 250 μL of 171.5 mM phosphatidylcholine, 250 μL of 32.3 mM cholesterol (corresponding to a molar ratio of 5.3:1 of phosphatidylcholine:cholesterol), and 500 μL of the 1 mM C_8. Then, this ethanolic solution was injected via a syringe coupled to a polytetrafluoroethylene tube (inner diameter of 0.8 mm, and outer diameter of 1.58 mm) into 9 mL of Milli-Q water under stirring using a NE-300 Just Infusion Syringe Pump (New Era Pump Systems, USA). The final liposomal dispersion was stored at room temperature in the dark.

The functionalization of the produced liposomes was achieved using the post-insertion method adapted from a previous publication [28]. The method consists in incubating 1 mg of liposomes with 1–3 nmol of AT11-TEG-Cholesteryl stock solution at room temperature for 20 min. To confirm the functionalization, an acrylamide gel was performed, with SYBR™Gold (Thermo Fisher Scientific™, Waltham, MA, USA) as the nucleic acid stain. HyperLadder™ 25 bp with 25–500 base pairs (Bioline) was used as a relative mobility marker. The obtained

AT11-functionalized liposome dispersions were stored at 4 °C until needed. The percentage of AT11-TEG-Cholesteryl anchored to the liposomes was also measured using a Horiba Fluoromax 4 fluorometer (Japan) by following the fluorescence of Cy5-AT11-TEG-Cholesteryl (Cy5, λ_{ex} = 650 nm and λ_{em} = 664 nm). For that, 1 mg of liposomes were incubated with 1–3 nmol of Cy5-AT11-TEG-Cholesteryl stock solution at room temperature for 20 min, and a centrifugal concentrator (Sartorius, Germany; MWCO of 100 kDa) was used to determine the amount of free aptamer that passed through the vertical membrane. Fluorescence intensities of the original samples (before the centrifugation) and of the free aptamer (that passed through the vertical membrane) were recorded and these values were used to calculate the percentage of the anchored Cy5-AT11-TEG-Cholesteryl (Table S1).

To calculate the encapsulation efficiency of the C_8-associated liposomes, a centrifugal concentrator (Sartorius, Germany; MWCO of 2 kDa) was used to determine the amount of free drug that passed through the vertical membrane. This free drug was then collected and measured with UV–Vis spectrophotometry (Thermo Scientific™Evolution 220, Waltham, MA, USA). The amount of C_8 was quantified using a calibration curve (y = 0.043x–0.0178; R^2 = 0.9988), which was constructed from measurements of samples with known concentrations (0.625 μM, 1.25 μM, 2.5 μM, 5 μM, and 10 μM) at 495 nm [29,30]. After determining the concentration of encapsulated C_8, the encapsulation efficiency (EE%) was calculated using the following equation:

$$EE\% = \frac{Quantified\ encapsulated\ mass\ of\ drug}{Initial\ mass\ of\ drug} \times 100$$

2.2.2. Characterization of the liposomes

The characterization of liposomes was made by Dynamic Light Scattering (DLS), determining the hydrodynamic dimensions and the zeta potential with a Zetasizer Nano ZS (Malvern Instruments, UK), using the Malvern Zetasizer software v7.13. The determinations were performed in triplicate by analysing 1 mL of liposome dispersion in a 1 cm plastic cuvette at 25 °C. The stability in terms of hydrodynamic diameter and PDI of the liposomes was recorded up to 7 weeks (for empty or C_8-associated liposomes) or up to 29 days (for AT11 liposomes with or without C_8).

The morphology of the liposomes was observed by transmission electronic microscopy (TEM), using a Hitachi HT7700 microscope. Briefly, liposome samples were placed on formvar-coated copper grids and allowed to dry at room temperature, then the images were acquired at a voltage of 80 kV [31] (Fig. S1).

Drug release kinetic of the C_8-associated liposomes was also assessed. Initially, a standard curve was generated (y = 72790x–45613; R^2 = 0.9834) with varying concentrations of C_8 solution (0.625 μM, 1.25 μM, 2.5 μM, 5 μM, and 10 μM), using a Horiba Fluoromax 4 fluorometer (Japan; λ_{ex} = 495 nm and λ_{em} = 510 nm). Subsequently, 100 μL of C_8-associated liposomes were placed in a Slide-a-Lyzer™ (Thermo Fisher Scientific™, Waltham, MA, USA; MWCO of 3.5 kDa). This dialysis device was inserted in an Eppendorf containing 1 mL of phosphate-buffered saline (PBS) solution. At various time points (5 min, 15 min, 30 min, 1 h, 2 h, 3 h, 4 h, 5 h, 6 h, 12 h, 24 h, 48 h, and 72 h), 100 μL of PBS solution was collected and replaced. The C_8-associated liposomes were kept under agitation at room temperature using a PTR-35 Multi-Rotator (Grant Instruments Cambridge, UK). The fluorescence of the collected samples was measured using the fluorometer, and these values were used to calculate the percentage of drug released.

2.2.3. In vitro studies

Nonmalignant epithelial cells isolated from the esophagus (Het1A; ref. CRL-2692™, ATCC) were grown in DMEM medium, supplemented with 10 % fetal bovine serum (FBS) and 1 % penicillin/streptomycin antibiotic. Squamous cell carcinoma of the tongue (UPCI-SCC-154; ref. ACC669, DSMZ) cells were grown in EMEM medium, supplemented with 1 × MEM non-essential amino acids and 10 % FBS and 1 % penicillin/streptomycin antibiotic. Both cell lines were maintained under a controlled humidified atmosphere at 37 °C and 5 % CO_2.

2.2.3.1. Cell viability. For MTT assay, UPCI-SCC-154 and Het1A cells were seeded in 96-well plates (5 × 10^4 cells/mL) and incubated overnight for cell adhesion. Then, cells were incubated with different concentrations of C_8 (0.05–5 μM), empty liposomes (0.36–71.26 μg/mL), C_8-associated liposomes (0.36–35.63 μg/mL of liposomes with 0.05–5 μM of C_8) and AT11 liposomes (3.56 μg/mL with or without 0.5 μM of C_8).

After the incubation period (24, 48 or 72 h), the medium was replaced with a fresh one containing MTT and further incubated at 37 °C for 4 h. The resulting formazan crystals were dissolved in DMSO, and the absorbance was recorded in a BioRad xMark™ microplate reader (Bio-Rad, Hercules, CA, USA) at 570 nm. Cell viability was normalized to the control condition (wells containing untreated cells).

For the medium replacement experiment, cells were incubated with the stimuli for 48 h, then the medium was replaced by a new one without any treatment for an additional 24 h. After that, cells were incubated with fresh medium containing MTT and further incubated at 37 °C for 4 h. The resulting formazan crystals were solubilized, and the absorbance was measured as described above.

Similar experiments were also conducted after treating the cells with AT11-TEG-Cholesteryl (35 nM) without (72 h of incubation) or with medium replacement (48 h of incubation with the stimuli and 24 h with fresh medium).

2.2.3.2. Western-blot. For nucleolin protein detection, UPCI-SCC-154 and Het1A cells were lysed, and total protein was quantified using a Pierce bicinchoninic acid protein assay Kit (Thermo Scientific) according to the manufacturer's instructions. Once quantified, 20 μg of total protein was heated for 5 min at 100 °C and then resolved on 10 % sodium dodecyl sulfate-polyacrylamide gel electrophoresis (SDS-PAGE). Thereafter, proteins were transferred to polyvinylidene difluoride filter (PVDF, Amersham Hybond P 0.45 μm PVDF, GE Healthcare) blotting membranes and blocked with a 5 % milk solution prepared in TBS-T (200 mM Tris-HCl, pH 7.6; 1.37 M NaCl; 0.1 % Tween 20) during 1 h. Next, primary anti-nucleolin polyclonal antibody (1:2000 in 0.5 % non-fat dry milk in TBS-T, ref PA3-16875, Thermo Scientific) incubation was performed overnight at 4 °C. Then, horseradish peroxidase (HRP)-labelled anti-rabbit IgG secondary antibody (1:5000 in TBS-T, ref 65–6120, Thermo Scientific) was incubated for 1 h at room temperature. Incubation with anti-β-actin antibody (1:5000 in 0.5 % of non-fat dry milk in TBS-T, ref MA1-140, Thermo Scientific) was also performed in the membranes during 2 h at room temperature. After that, HRP-labelled anti-mouse IgG secondary antibody (1:5000 in TBS-T, ref 31430, Thermo Scientific) incubation was performed for 1 h at room temperature. In the end, the membrane was incubated with enhanced chemiluminescence substrate (WesternBright™ Sirius, K-12043-D10, Advansta) and images were obtained with the ChemiDoc™ XRS system (BioRad, Hercules, CA, USA) and analyzed using Image Lab (BioRad, Hercules, CA, USA).

2.2.3.3. Cell uptake and nucleolin staining. The uptake assays were performed by fluorescence confocal microscopy; Het1A and UPCI-SCC-154 cells were seeded at 5 × 10^4 cells/mL in a treated μ-slide eight well (IBIDI, Gräfelfing, Germany) in 200 μL of medium.

For nucleolin immunocytochemistry, UPCI-SCC-154 and Het1A cells were incubated with primary anti-nucleolin polyclonal antibody (PA3-16875, Invitrogen, Waltham, MA, USA) at 1:100 for 2 h and a secondary antibody (Alexa Fluor 488®; dilution of 1: 1000) for 1 h [32]. Nuclei were stained with the nuclear probe Hoechst 33342 for 15 min. The cells were imaged using a Zeiss AxioObserver LSM 710 microscope and the 40× objective was used to capture the fluorescence images.

UPCI-SCC-154 and Het1A cells were incubated with 2 μM of the

nuclear probe Hoechst 33342 for 15 min. Then, the wells were washed 3 times with PBS and treated with AT11 liposomes (3.56 μg/mL with 0.5 μM of C_8) for 2 h. Cells were imaged using a Zeiss AxioObserver LSM 710 microscope (Oberkochen, Germany) with 405 and 488 nm laser excitation for Hoechst 33342 and C_8, respectively. Similar experiments were conducted with Cy5-labelled AT11 liposomes (3.56 μg/mL) and the cells were imaged with 405 and 633 nm laser excitation for Hoechst 33342 and AT11, respectively.

2.2.3.4. Cell proliferation and death assays. For the cell proliferation assay, Het1A and UPCI-SCC-154 cells were seeded at 5×10^4 cells/mL in 24 well plates with glass coverslips. After 24 h of incubation, cells were treated with empty liposomes, C_8-associated liposomes, AT11 empty liposomes or AT11C_8-associated liposomes for 24 h. After that, cells were washed with phosphate-buffered saline (PBS), fixed with 4 % paraformaldehyde (PFA) at room temperature for 10 min, permeabilized for 5 min with 1 % Trinton X-100 and blocked for 1 h with PBS containing 20 % FBS. Then cells were incubated overnight at 4 °C with a rabbit primary antibody anti-ki67 (ab16667, Abcam; 1:200) in PBS with 0.1 % of Tween-20 (PBS-T) containing 1 % FBS. Next, cells were washed with PBS-T and incubated with secondary antibody goat anti-rabbit Alexa Fluor® 647 (1:1000) at room temperature for 1 h in PBS-T containing 1 % FBS. Nuclei were stained with Hoechst 33342 (2 μM) for 10 min, and coverslips were placed on glass slides using fluorescence mounting medium (Dako, Germany). Images were then acquired on a LSM710 confocal laser scanning microscope (Carl Zeiss) at a 40× magnification. Fluorescence images were processed using Zen software (Carl Zeiss).

Propidium iodide (PI; 5 1 mg/mL; Sigma-Aldrich) was used to quantify the number of dying cells, using a dye exclusion method [33]. For this assay, Het1A and UPCI-SCC-154 cells were seeded at 5×10^4 cells/mL in treated μ-slide eight well (IBIDI, Gräfelfing, Germany). Both cells were treated with empty liposomes, C_8-associated liposomes, AT11 empty liposomes or AT11C_8-associated liposomes for 24 h and then, rinsed with PBS. Hereafter, cell nuclei were stained with Hoechst 33342 (2 μM) for 10 min, washed with PBS and then PI (2 μg/mL) was added to the cells for 15 min. Three random microscopic fields were acquired per replicate using an Axio Observer Z1 (Carl Zeiss) at a 40× magnification. The number of PI-positive cells was obtained using the ImageJ software.

2.2.3.5. Caspase-3 activity assay. Caspase-3 activity was estimated by a colorimetric method using a commercial kit (CAT no. E-CK-A311, Elabscience) and according to the manufacturer's protocol. Briefly, 100×10^4 cells were seeded in a t-flask of 25 cm^2. The day after, the cells were treated with different stimuli (control, AT11 empty liposomes or AT11C_8-associated liposomes) for 24 h. The cells were then collected and 50 μL of cold lysis buffer was added to the resulting cell pellet. The total protein was quantified with Pierce™ BCA Protein Assay Kit according to the manufacturer's protocol. A 2 × reaction working solution (50 μL) was added to the wells of a 96-well plate. Then, 45 μL of sample homogenate (containing 100 μg of protein) was added to the sample wells, and 45 μL lysis working solution was added to the blank wells. Finally, 5 μL of Ac-DEVD-pNA was added and thoroughly mixed. The mixture was incubated for 4 h at 37 °C. Absorbance was observed at 405 nm by a BioRad xMark™ microplate reader (BioRad, Hercules, CA, USA). Caspase-3 activity was calculated by using the formula:

$$Caspase\ 3\ activity = \frac{\left(OD_{sample} - OD_{blank}\right)}{\left(OD_{negative\ control} - OD_{blank}\right)} \times 100$$

2.2.3.6. Cell migration. For the cell migration assay, the *in vitro* scratch assay was performed [34]. For that, UPCI-SCC-154 cells were seeded at 10×10^4 cells/mL in 12-well plates for 24 h. Then, a linear scratch was created in the cells with a sterile 200 μL micropipette tip, and the detached cells were removed by rinsing with PBS. The remaining cells were incubated with EMEM containing the different stimuli (control, AT11 empty liposomes or AT11C_8-associated liposomes). Cell migration into the scratched region was recorded at 0, 24 and 48 h using an inverted microscope (Axio Observer Z1, Carl Zeiss). Images were analyzed using ImageJ software.

2.2.3.7. Cell invasion. The invasion capability of oral cancer cells was assessed using 24-well Corning® BioCoat™ Factor Reduced Matrigel® Invasion Chamber as recommended by the manufacturer with some modifications [35]. Cells (5×10^4 cells/mL) were resuspended in serum-free medium and then 500 μL of the cell suspension was plated in the upper chamber of the transwell containing an 8-mm pore size PET membrane with Matrigel-coated membrane matrix. EMEM containing 10 % FBS (750 μL) was added to the lower chamber. The different conditions (control, AT11 empty liposomes or AT11C_8-associated liposomes) were introduced into both chambers. After 24 h of incubation, the cells in the upper chamber were removed with cotton swabs. The invading cells on the lower membrane surface were fixed in 4 % PFA for 10 min and stained with Hoechst 33342 (2 μM) for 10 min. Then, the invaded cells were observed by an Axioimager A1(Carl Zeiss) at a 5× magnification. Representative images were obtained by an AxioImager Z2 (Carl Zeiss) at a 20× magnification.

2.3. Statistical analysis

The data are presented as the mean ± standard of the error mean (SEM). Statistical analysis was performed using GraphPad Prism v.8.0.1 software (GraphPadSoftware, USA), employing analysis of variance (ANOVA) followed by Tukey's Multiple Comparison Test and unpaired *t*-test. Data were considered statistically significant when $p < 0.05$.

3. Results and discussion

Liposomes represent widely employed formulations for specialized drug delivery, due to their biocompatibility, biodegradability, and toxicological safety [15]. While several lipids can be employed for liposomes' preparation, phosphatidylcholine is the most commonly used [36]. In this work, the commercially available phosphatidylcholine, Phospholipon® 90G, was used to produce liposomes in combination with cholesterol, which enhances the structure stabilization and rigidity, by increasing the hydrophobic–hydrophobic interactions in the liposome's bilayer [37]. Specifically, liposomes were employed to obtain a more efficient delivery of C_8, which lacks selectivity for cancer cells [26]. Phospholipid vesicles were prepared by ethanol injection, which represents a simple, rapid, and reproducible method to prepare liposomes [38]. Previous reports have indicated that functionalizing liposomes with AS1411 can enhance their selectivity for cancer cells [39,40], which overexpress nucleolin in the cells' surface. This strategy was also used to overcome the efflux-mediated multidrug resistance effect, by favouring their uptake via receptor-mediated endocytosis [40]. Herein, the AS1411 derivative, AT11, was used as an alternative due to its improved anti-proliferative effect and nucleolin affinity [23]. Therefore, the obtained liposomal formulation was functionalized with AT11-TEG-Cholesteryl via the post-insertion method.

Empty liposome, both with or without AT11 conjugation, as well as C_8-associated liposomes (without AT11) were used as control conditions to better understand the potential of the produced liposomes.

Liposomes were characterized by DLS, to evaluate their size and surface potential (Table 1). As expected, AT11 conjugation increases in the liposomes' size, indicating that the hydrophilic molecule anchored to the outer surface of the vesicles has enlarged the hydrodynamic diameter. All the produced liposomes have a mean diameter comprised between 130 and 140 nm and dispersity below 0.3 [37], with a spherical morphology as observed in TEM images (Fig. S1). Additionally, both non-functionalized and AT11-functionalized liposomes seem to be stable

Table 1
Average size (Z-average), dispersity (Đ) and Zeta-potential of the produced liposomes. The results show the mean and standard deviation of three measurements (mean ± SD).

	Z-average (nm)	Đ	Zeta-Potential (mV)
Empty liposomes	132.6 ± 0.8	0.14	−6.1 ± 1.2
AT11 empty liposomes	135.9 ± 1.3	0.14	−11.4 ± 4.8
C_8-associated liposomes	130.1 ± 0.7	0.12	12.0 ± 1.2
AT11 C_8-associated liposomes	133.1 ± 1.1	0.12	−11.3 ± 2.1

for up to 7 weeks or 29 days, respectively (Fig. S2), with a tendency to decrease the hydrodynamic diameter over time. As expected, the presence of the negatively charged aptamer led to a reduction in the liposomes' surface potential [40]. Importantly, the ethanol injection method achieved a very high C_8-association efficiency, consistently over 95 % (98.24 % ± 1.21, indicated as mean ± SEM). Furthermore, the produced liposomes were able to release up to 86.2 % of C_8 after 72 h (Fig. S3), indicating efficient release. These results are promising for potential local applications, suggesting that the liposomes can rapidly release the compound at the targeted tissue.

To confirm the post-insertion of AT11 aptamer to the surface of the liposomes, fixed amounts of liposomes (1 mg) were incubated with two different amounts of the AT11-TEG-Cholesteryl aptamer (1 or 3 nmol) and then analyzed by acrylamide gel with SYBR™Gold staining (Fig. S4). Free AT11 was used as a control (lane 1) for comparison. As observed, the anchoring of the lipophilic cholesteryl to the liposomes prevented AT11 from migrating, resulting in a reduction of the AT11 band intensity. These data strongly indicated the successful anchoring of the aptamer into the liposomes bilayer. Additionally, due to the hydrophilic characteristics and considerable size of the aptamer it compels it to reside on the outer surface of the liposomes [28]. The functionalization efficiency was also determined by tracking the presence of Cy5-AT11-TEG-Cholesteryl after the post-insertion method. As presented in Table S1, the aptamer was attached to the liposomes around 99 %.

After production, the *in vitro* performances of liposomes as formulation for the delivery of C_8 were analyzed, by different biological tests, on an oral cancer cell line (UPCI-SCC-154) and a nonmalignant epithelial cell line of the esophagus (Het1A).

Evidence suggests that G-rich sequences capable of forming G4s could serve as potential anticancer targets [16]. The stabilization of these sequences, which were identified in the promoter regions of prominent oncogenes (e.g. c-MYC and KRAS) can modulate key mechanisms associated with cancer development, including gene transcription and translation [16]. Therefore, the use of compounds promoting the formation of G4s represents a possible therapeutic strategy; an example of such molecules is the acridine orange derivative C_8, which was previously used to stabilize a sequence found in the KRAS promoter (KRAS-22RT) [26]. However, the compound was also associated with off-target effects, presenting high toxicity in normal cells. The cytotoxic activity of this compound was already characterized in some cancer cell lines and normal human dermal fibroblasts [26,32]. Nevertheless, in this work, for a better understanding of its effects on the viability of the cell lines used in this work, different concentrations were tested after 24, 48 or 72 h of incubation. As observed in Fig. S5, and consistent with the results described in other works [26,32], the cytotoxicity of the compound is almost the same in nonmalignant and cancer cells. Therefore, a strategy to improve the selectivity of the compound, such as using liposomal delivery, is needed to minimize the toxicity of C_8 towards nonmalignant cells.

The cytocompatibility of the produced empty liposomes was evaluated by testing a range of concentrations and analyzing their effect on cell viability after 24, 48 or 72 h of incubation. As observed in Fig. S6, liposomes did not affect significantly the viability of both cancer (UPCI-SCC-154) or nonmaligant (Het1A) cells up to the concentration of 53.6 μg/mL. For that reason, C_8-associated liposomes were tested up to this dose. As observed in Fig. S7 and Fig. 1A, a dose-response effect was observed both in nonmalignant and cancer cell lines; thus, the association of the compound in the liposomes did not improve the off-target effects of C_8. For the following assays, a C_8's final concentration of 0.5 μM was considered for a better comparison with the other studies in which this compound was delivered through association with different G4 aptamer-based drug delivery systems [31].

Hence, to improve the selectivity of the C_8-associated liposomes, AT11 was used as a targeting moiety. As presented in Fig. S8 and Fig. 1B, some selectivity of the liposomes towards oral cancer cells was achieved, reflected in a difference of about 20 % in the viability of the two cell lines at the same conditions. However, increasing the amounts of AT11 in the liposomes did not improve selectivity, as observed in Fig. S8. Therefore, the optimal prescription for AT11-TEG-Cholesteryl insertion in liposomes was defined as 1 nmol of AT11-TEG-Cholestyl per 1 mg of liposomes, and the subsequent experiments were conducted with this ratio. Improved selectivity was achieved, as reported in previous studies, which demonstrated that liposomes functionalized with AS1411 enhanced drug delivery to cancer cells [39–41]. Since AT11 is an AS1411 derivative targeting the same protein (nucleolin), similar improvements in selectivity were expected.

Previous reports have also suggested that AS1411 aptamer is cleared from nonmalignant cells, but is retained in cancer cells [32,42,43]. Therefore, a new experiment was carried out in which, after 48 h of incubation with the stimuli, the medium was replaced by a new one (without any additional liposomes). Under these conditions, as observed in Fig. 1C, the toxicity of AT11 C_8-associated liposomes was minimized in the nonmalignant cell line (cell viability went from around 60 % to around 80 %), while in the cancer cell line was maintained at about 40 %. Moreover, the cytotoxic effect of the AT11 empty liposomes was eliminated. Previously, in other studies performed by our group with aptamer-based drug delivery systems, a cytotoxic effect associated with aptamers was observed, although the concentrations used were higher (5–15 μM; in this case, AT11 is at a 35 nM concentration) [18,23,31,32]. Consistent with the results from this work with the AT11 liposomes, other authors have also reported that AS1411-functionalized nanoparticles did not affect cell viability. This was attributed to the low concentrations of the aptamer, which served primarily as a targeting moiety, enhancing the selectivity of the nanoparticles for cancer cells [39,44].

Additionally, to verify if the decrease in cell viability observed in Fig. 1B and 1C was due to the anticancer effect of AT11 itself or if there was an additional decrease attributable to increased selectivity by the AT11 aptamer, MTT assay was performed after treating the cells with AT11 at 35 nM. As shown in Fig. S9 no significant changes were induced after this stimulus (with or without medium replacement), suggesting that the observed effect was due to the increased selectivity by the AT11 aptamer.

As already mentioned, previously it was reported that the target of AT11 aptamer is nucleolin, whose expression and location in tumor cells are anomalous compared to nonmalignant cells and are correlated with increased cancer aggressiveness [45]. Additionally, it was demonstrated that UPCI-SCC-154 cells express more nucleolin and that is more located on the cell's surface than in a nonmalignant cell line (normal human dermal fibroblasts) [19]. Nevertheless, the expression of this protein was also analyzed to confirm whether it presents higher expression in the cancer cell line compared to the nonmalignant cell line used in this work (Het1A). As observed in Figs. S10 and S11, the UPCI-SCC-154 expresses more nucleolin on their cell membrane compared to Het1A cells. Thus, the observed selectivity towards the UPCI-SCC-154 cell line is likely due to the higher expression of this protein in this cell line.

Then, the internalization of AT11 C_8-associated liposomes was assessed by confocal microscopy in UPCI-SCC-154 and Het1A cell lines. For this experiment, the intrinsic fluorescence of C_8 was used for the liposomes tracking. Additionally, Hoechst 33342 was used to stain the

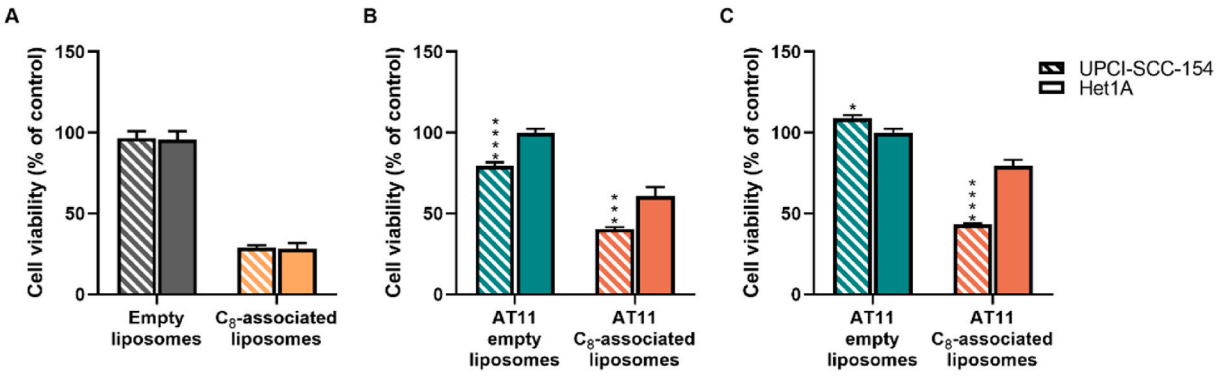

Fig. 1. MTT cell viability assays in UPCI-SCC-154 (columns with pattern) and Het1A (columns without pattern) cell lines of (A) empty liposomes or C_8-associated liposomes after 72 h of incubation, (B) AT11 empty liposomes or AT11 C_8-associated liposomes after 72 h of incubation and (C) AT11 empty liposomes or AT11 C_8-associated liposomes after 48 h of incubation with the stimuli and 24 h with fresh medium. *$p < 0.05$, ***$p < 0.001$ and ****$p < 0.0001$ when compared to Het1A cell line using the using unpaired two tailed *t*-test.

cell nuclei. As shown in Fig. 2 and Table S2, and as expected, the liposomes are more internalized by the malignant cell line, confirming the improved selectivity of the drug delivery system towards the cells of interest. Similar experiments were conducted with AT11 empty liposomes in which a higher uptake of the liposomes was also observed in the cancer cell line (Fig. 3, Table S2).

Then, to better understand the potential anticancer effect of the produced liposomes, their impact on cell proliferation was assessed using ki67 immunostaining. This nuclear marker, which is present throughout all active phases of the cell cycle (G1, S, G2 and M), is commonly used to study cell proliferation. Moreover, ki67's high expression is associated with tumor aggressiveness, metastasis and poor response to chemotherapy [46]. As observed in Fig. 4, the AT11 C_8-associated liposomes induced a significant reduction in the percentage of cells positive for this protein in the UPCI-SCC-154 cell line, suggesting that the produced liposomes may disrupt replication in oral cancer cells. Additionally, this assay was performed with plain liposomes (without AT11 functionalization) and there were no significant differences between the two cell lines in each condition (Fig. S12), suggesting that the selectivity obtained with the AT11 functionalized liposomes (observed in Fig. 4) was derived from the selectivity conferred by the aptamer.

Furthermore, two indicators of cell death were utilized to evaluate whether cell death was also induced, namely through internalization of PI in non-permeabilized cells and the caspase-3 levels. As observed in Fig. 5, treating the cells with the AT11C_8-associated liposomes significantly increased PI internalization by the malignant cells. Since PI is a membrane-impermeant nucleic acid intercalator, this result suggests that the cell membrane is compromised, allowing the molecule to penetrate the cells and intercalate into the nuclear DNA. Similar experiments were performed with plain liposomes in which no significant differences were observed between the two cell lines in the tested conditions (empty liposomes and C_8-associated liposomes; Fig. S13).

Additionally, as demonstrated in Fig. 6, AT11-functionalized liposomes increased caspase 3 levels, which is an executor of the apoptosis pathway and responsible for cell disintegration [47]. Overall, these results along with the ki67 immunostaining, suggest that the AT11 C_8-associated liposomes can selectively decrease proliferation and induce cell death in the tongue cancer cell line, which may be due to the targeting conferred by the aptamer insertion in the liposomes.

In oral cancer patients diagnosed at an advanced stage, there is an increased likelihood of invasion into neighboring tissues and a high risk

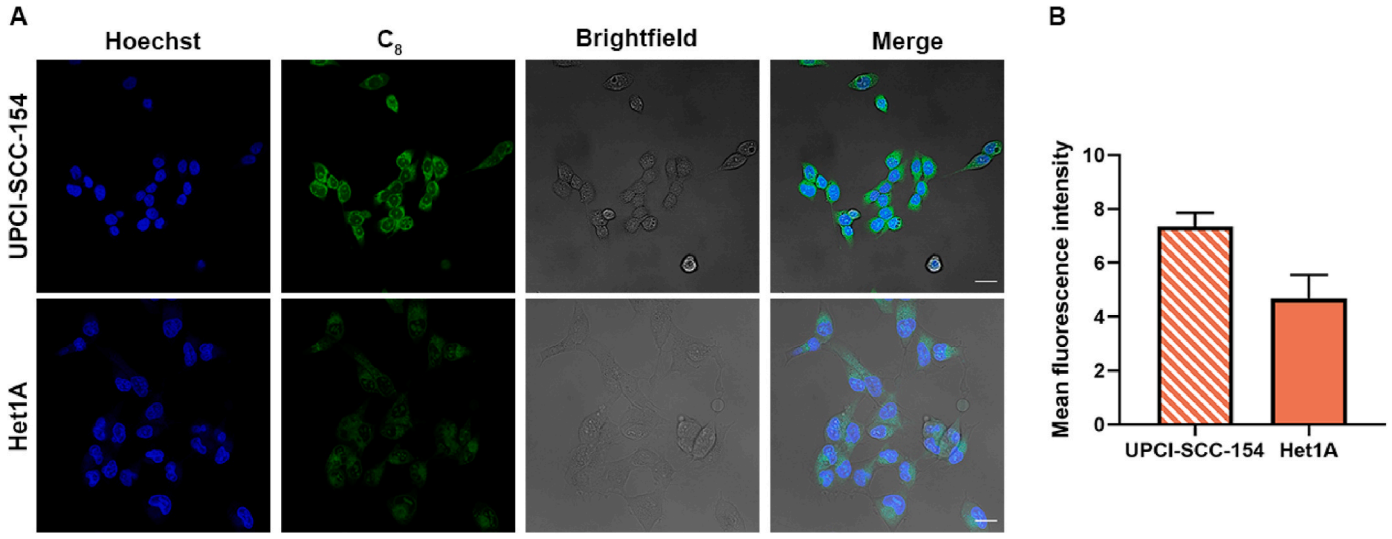

Fig. 2. – (A) Fluorescence confocal microscopy images of UPCI-SCC-154 and Het1A cells incubated with AT11 C_8-associated liposomes for 2 h. Cell nuclei are stained with Hoechst 33342 in the blue channel while C_8 emits green fluorescence. Scale bar: 20 μm. (B) Mean fluorescence intensity obtained by fluorescence confocal microscopy of green channel AT11C_8-associated liposomes in UPCI-SCC-154 (column with pattern) and Het1A (columns without pattern) cells after 2 h incubation. Values are presented as mean values ± standard error mean (SEM). (For interpretation of the references to color in this figure legend, the reader is referred to the Web version of this article.)

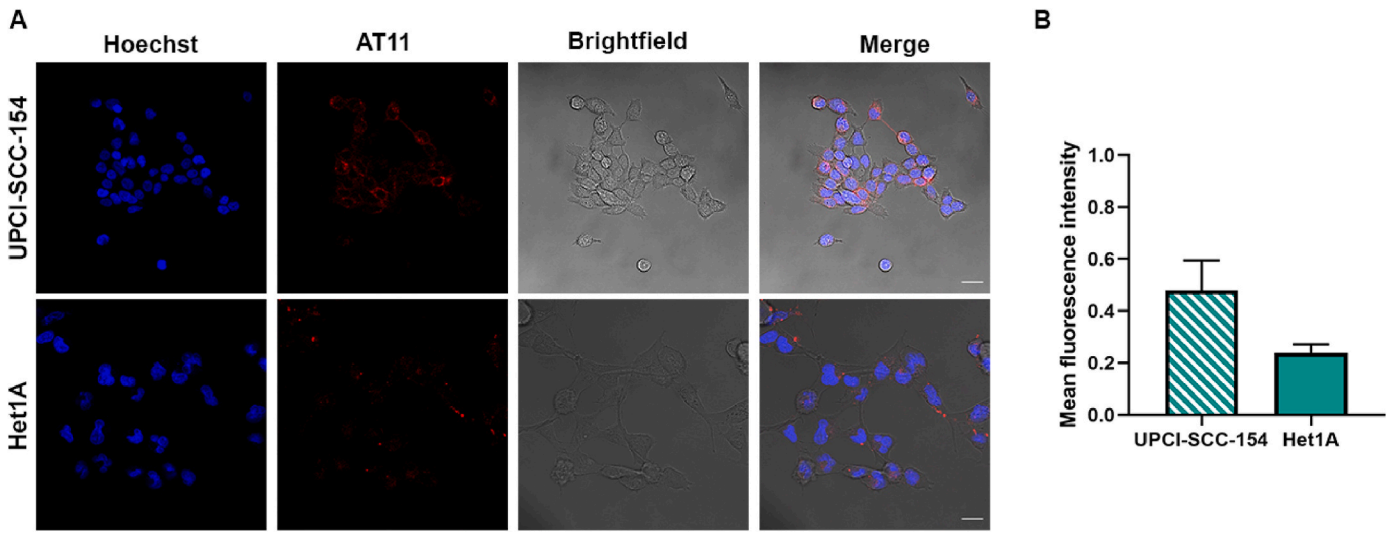

Fig. 3. – (A) Fluorescence confocal microscopy images of UPCI-SCC-154 and Het1A cells incubated with AT11 empty liposomes for 2 h. Cell nuclei are stained with Hoechst 33342 in the blue channel while AT11 is labelled with a Cyanine5. Scale bar: 20 μm. (B) Mean fluorescence intensity obtained by fluorescence confocal microscopy of AT11 empty liposomes in UPCI-SCC-154 (column with pattern) and Het1A (column without pattern) cells after 2 h incubation. Values are presented as mean values ± standard error mean (SEM). (For interpretation of the references to color in this figure legend, the reader is referred to the Web version of this article.)

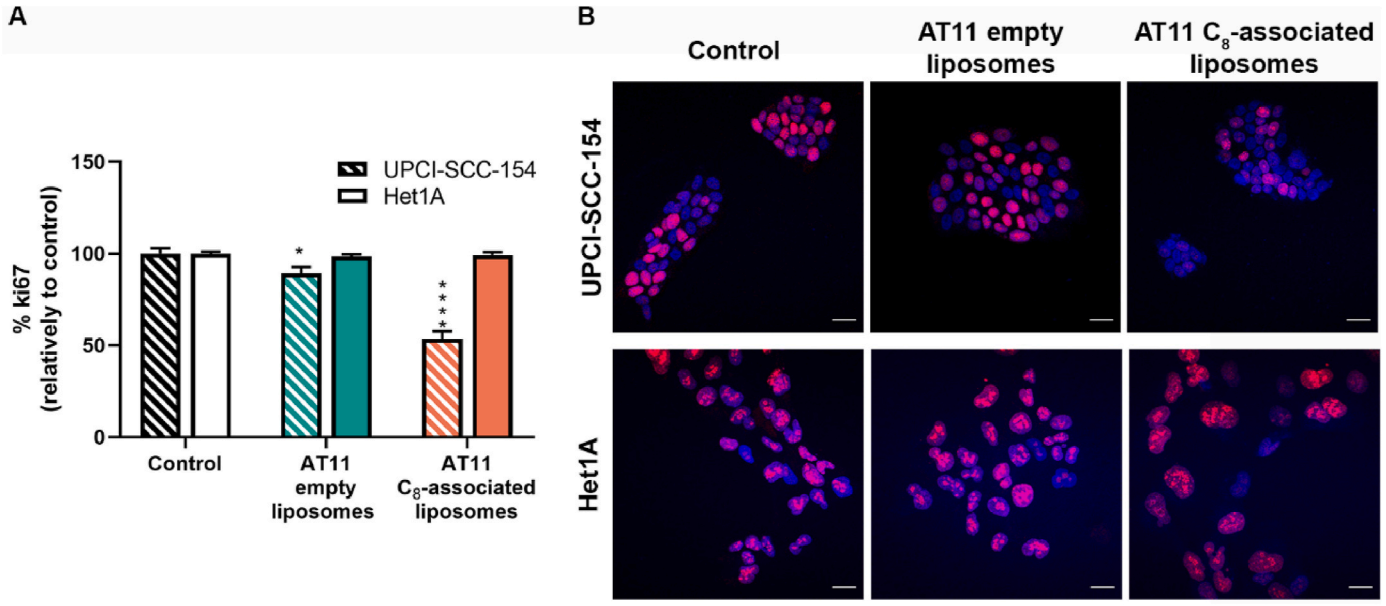

Fig. 4. – (A) Percentage of ki67 positive cells in UPCI-SCC-154 (columns with pattern) and Het1A (columns without pattern) cell lines after 24 h of different treatments (control, AT11 empty liposomes or AT11 C_8-associated liposomes). *p < 0.05 and ****p < 0.0001 when compared to Het1A cell line using the unpaired two tailed *t*-test. (B) Representative images of control, AT11 empty liposomes or AT11 C_8-associated liposomes conditions in UPCI-SCC-154 and Het1A cell lines after 24 h of stimuli. Nuclei are shown in blue and ki67 in red. Scale bar: 20 μm. (For interpretation of the references to color in this figure legend, the reader is referred to the Web version of this article.)

of developing a second malignancy during patient's lifetime [48]. Cancer metastasis involves a multi-step process, including detachment from the primary tumor site, followed by migration and invasion [49]. The current treatment options face some challenges due to these two key steps, which can cause metastasis and tumor recurrence [50]. Therefore, the effect of the liposomes on the migration and invasion mechanisms of the oral cancer cell line was evaluated to understand how these processes are affected.

Firstly, the cell scratching assay was carried out to investigate the inhibitory ability of the AT11 C_8-associated liposomes in cell migration. The migration of the cells through the scratch was recorded for up to 48 h. As observed in Fig. 7, there is a slight slowdown in the migration capacity after treatment with AT11 empty liposomes, which can be related to the aptamer. However, treatment with AT11 C_8-associated liposomes resulted in a significant impairment in the migration of the cells towards the scratch, which can be attributed to the compound in liposomes.

Additionally, and since cells need to penetrate the basement membrane for efficient metastasis [51], the effect of the liposomes on the invasiveness of the oral cancer cell line was also evaluated. As observed in Fig. 8, there was a clear decrease in the ability of these cells to invade the Matrigel after treatment with AT11C_8-associated liposomes. Therefore, the compromised migration was accompanied by reduced invasion of UPCI-SCC-154 cell line, suggesting that these liposomes may decrease

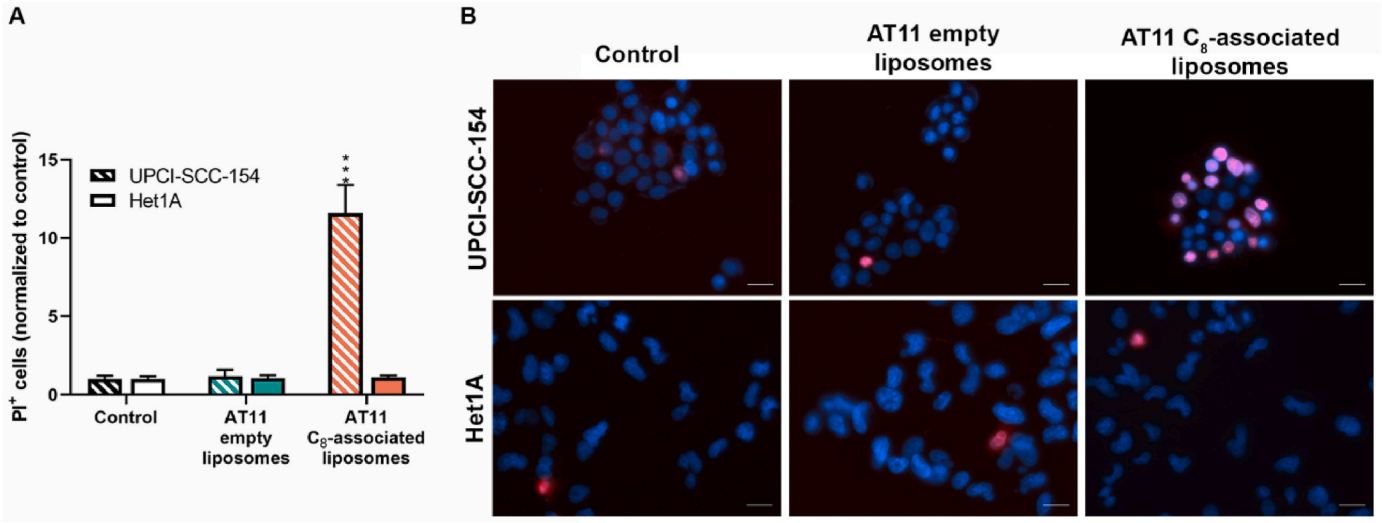

Fig. 5. – (A) Propidium iodide (PI) positive cells (normalized to control) in UPCI-SCC-154 (columns with pattern) and Het1A (columns without pattern) cell lines after 24 h of different treatments (control, AT11 empty liposomes or AT11C_8-associated liposomes). ***$p < 0.001$ when compared to Het1A cell line using unpaired two-tailed *t*-test. (B) Representative images of control, AT11 empty liposomes or AT11 C_8-associated liposomes conditions in UPCI-SCC-154 and Het1A cell lines after 24 h of stimuli. Nuclei are shown in blue and PI in red. Scale bar: 20 μm. (For interpretation of the references to color in this figure legend, the reader is referred to the Web version of this article.)

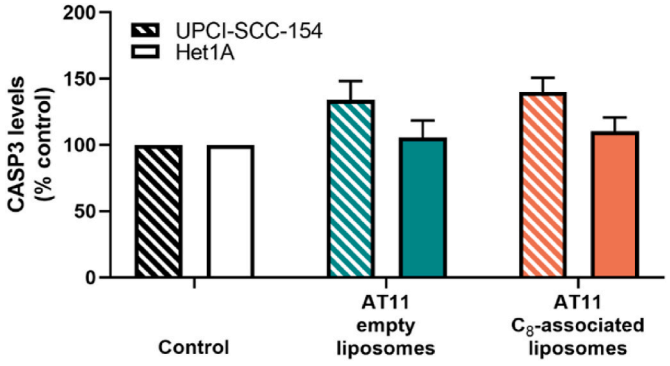

Fig. 6. Percentage of caspase 3 (CASP3) levels (relatively to control) in UPCI-SCC-154 (columns with pattern) and Het1A (columns without pattern) cell lines after 24 h of different treatments (control, AT11 empty liposomes or AT11 C_8-associated liposomes).

the cell's metastatic ability.

Overall, AT11 C_8-associated liposomes seem to be a promising strategy for oral cancer treatments. However, in the future, *in vivo* studies are needed to evaluate the pharmacokinetics, biodistribution, and therapeutic potential in a more complex environment. For that, xenograft models (for instance, obtained by injecting UPCI-SCC-154 cells [52]) or immunocompetent HPV16 transgenic model (which develops lesions in the head and neck regions [53]) could be relevant options for a more accurate assessment of the produced liposomes. Moreover, the transgenic model could be a promising option since it closely resembles human disease and avoids overlooking crucial immune system interactions [54,55].

Regarding future clinical applications, and considering the accessibility of oral cancers, it could be beneficial to administer liposomes through local application by using intraoral systems (such as fast-dissolving oral films, mucoadhesive gels or adhesive patches) [56], potentially reducing side effects. Additionally, AT11 functionalization will provide selectivity towards nucleolin-overexpressing cancer cells, which is expected to minimize toxicity in the surrounding tissues.

4. Conclusions

In this contribution, the production of C_8-associated liposomes functionalized with AT11-TEG-Cholesteryl is described aiming for more selective delivery of cytotoxic compounds towards the oral cancer cell line, UPCI-SCC-154.

The liposomes were produced by the ethanol injection method, presenting hydrodynamic diameters in the range of 130–136 nm with a dispersity under 0.3. This suggests that the method is suitable for the production of liposomes intended for drug delivery. The AT11 moiety was also efficiently post-anchored to the liposomal surface, as verified by acrylamide gel electrophoresis.

The empty liposomes exhibited cytocompatibility up to the concentration of 53.6 μg/mL and, when loaded with C_8, they did not improve the lack of selectivity of the compound, maintaining the high toxicity in the nonmalignant cell line. However, AT11 functionalization improved cancer selectivity. Moreover, experiments with fresh medium replacement, suggested that AT11 acts as a targeting moiety rather than a therapeutic molecule, as the effect on cell viability after 72 h of incubation with the AT11 empty liposomes was neutralized. The selectivity towards the oral cancer cell line was also confirmed by confocal microscopy, demonstrated by higher intrinsic fluorescence intensity of C_8 in these cells.

Regarding the effects of AT11 C_8-associated liposomes on certain cell death mechanisms, we observed that they induced cancer cell death (demonstrated by an increase of PI-positive cells and higher caspase 3 levels). Furthermore, these liposomes reduced cancer cell proliferation, evidenced by a decrease in the number of ki67-positive cells, and inhibited migration (tested with a cell scratching assay) and invasion (evaluated using Matrigel-coated invasion chambers).

In conclusion, AT11-functionalized liposomes loaded with C_8 can promote a more selective effect of the compound towards oral cancer cells. Altogether, the reported results emphasize the potential of this compound as an anticancer agent, particularly when delivered selectively through the use of AT11-functionalized liposomes, as shown herein with the targeting of UPCI-SCC-154 cells.

CRediT authorship contribution statement

Jéssica Lopes-Nunes: Writing – review & editing, Writing – original

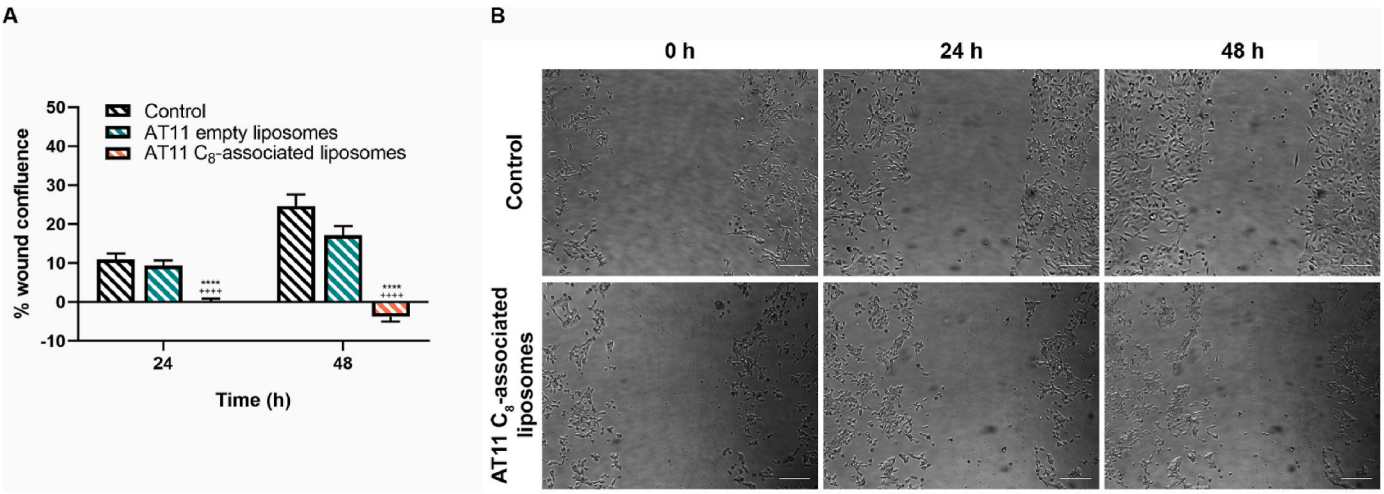

Fig. 7. – (A) Percentage of wound confluence at 0, 24, and 48 h postinjury in UPCI-SCC-154 with different treatments (control, AT11 empty liposomes or AT11 C_8-associated liposomes). ****$p < 0.0001$ when compared control and $^{++++}p < 0.0001$ when compared to AT11 empty liposomes using the one-way ANOVA, followed by the Tukey's multiple comparison test. (B) Representative images of control or AT11C_8-associated liposomes at 0, 24, and 48 h postinjury. Scale bar: 200 μm.

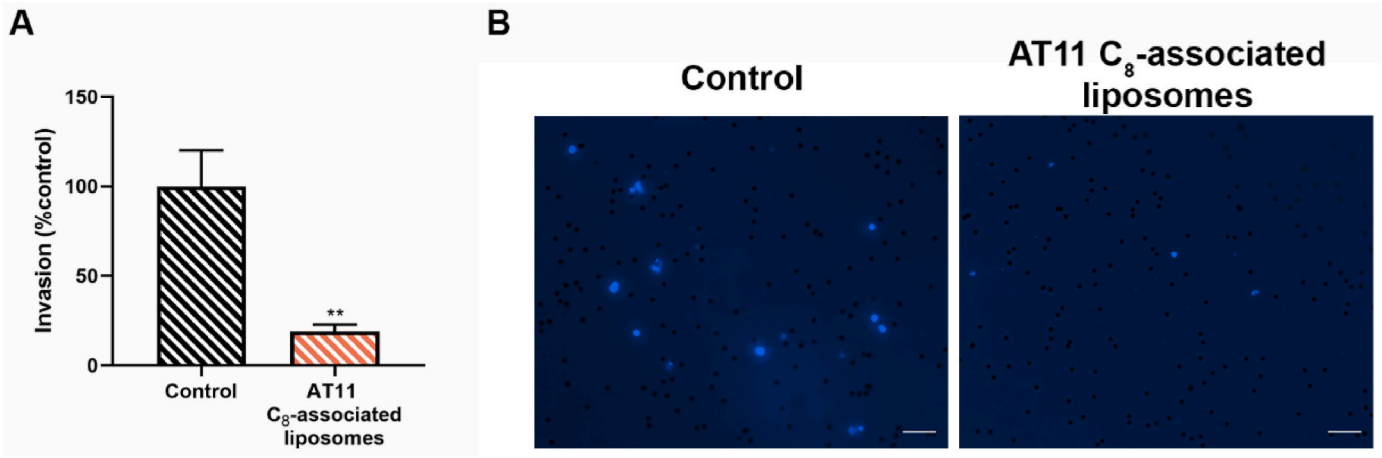

Fig. 8. – (A) Percentage of invading UPCI-SCC-154 cells after treatment with AT11 C_8-associated liposomes (normalized to control). **$p < 0.01$ when compared to control using the unpaired two tailed *t*-test. (B) Representative images of control or AT11C_8-associated liposomes conditions. Scale bar: 50 μm.

draft, Methodology, Investigation, Formal analysis, Data curation. **Maria Paula Cabral Campello:** Writing – review & editing, Methodology, Investigation. **António Paulo:** Writing – review & editing, Methodology, Formal analysis. **Claudio Nastruzzi:** Writing – review & editing, Methodology, Investigation, Formal analysis, Data curation. **Paula A. Oliveira:** Writing – review & editing, Methodology. **Carla Cruz:** Writing – review & editing, Validation, Supervision, Project administration, Methodology, Investigation, Funding acquisition, Formal analysis, Data curation, Conceptualization.

Declaration of competing interest

The authors declare that they have no known competing financial interests or personal relationships that could have appeared to influence the work reported in this paper.

Data availability

No data was used for the research described in the article.

Acknowledgements

Jéssica Lopes-Nunes acknowledges a doctoral fellowship grant from FCT ref. 2020.05329.BD (with DOI: 10.54499/2020.05329.BD, https://doi.org/10.54499/2020.05329.BD). Carla Cruz acknowledges the project ref. CENTRO-01-0145-FEDER-181235 funded by CENTRO 2020, through Fundo Europeu de Desenvolvimento Regional ref. CENTRO-01-0246-FEDER-000044 and collaborative project PAPILOMA DOI 10.54499/UIDP/00709/2020 (https://doi.org/10.54499/UIDP/00709/2020). Thanks are due to FCT/MCT for the financial support to the CICS-UBI UIDB/00709/2020 research unit, DOI 10.54499/UIDB/00709/2020 (https://doi.org/10.54499/UIDB/00709/2020), program funding with DOI 10.54499/UIDP/00709/2020 (https://doi.org/10.54499/UIDP/00709/2020) and to the CITAB-UTAD research unit under the project UIDB/04033/2020 (https://doi.org/10.54499/UIDB/04033/2020), POCI-01-0145-FEDER-022122 research unit, PPBI—Portuguese Platform of BioImaging, and to the Portuguese NMR Network (ROTEIRO/0031/2013-PINFRA/22161/2016), through national funds and, where applicable, co-financed by the FEDER through COMPETE 2020, POCI, PORL, and PIDDAC. C2TN/IST authors, MPC Campello and A Paulo, gratefully acknowledge the FCT support through the UID/Multi/04349/2019. This work was supported by EATRIS, the

European infrastructure for translational medicine.

This article/publication is based upon work from COST Action CA 17140 “Cancer Nanomedicine from the Bench to the Bedside” supported by COST (European Cooperation in Science and Technology).

Appendix A. Supplementary data

Supplementary data to this article can be found online at https://doi.org/10.1016/j.jddst.2024.106214.

References

[1] R.L. Siegel, K.D. Miller, N.S. Wagle, A. Jemal, Cancer statistics, Ca - Cancer J. Clin. (2023), https://doi.org/10.3322/caac.21763, 2023.
[2] J.H. Ng, N.G. Iyer, M.H. Tan, G. Edgren, Changing epidemiology of oral squamous cell carcinoma of the tongue: a global study, Head Neck (2017), https://doi.org/10.1002/hed.24589.
[3] X.J. Chen, X.Q. Zhang, Q. Liu, J. Zhang, G. Zhou, Nanotechnology: a promising method for oral cancer detection and diagnosis, J. Nanobiotechnol. (2018), https://doi.org/10.1186/s12951-018-0378-6.
[4] J.E. Heck, J. Berthiller, S. Vaccarella, D.M. Winn, E.M. Smith, O. Shan'gina, S. M. Schwartz, M.P. Purdue, A. Pilarska, J.E. Eluf-Neto, A. Menezes, M.D. McClean, E. Matos, S. Koifman, K.T. Kelsey, R. Herrero, R.B. Hayes, S. Franceschi, V. W. Wünsch-Filho, L. Fernández, A.W. Daudt, M.P. Curado, C. Chen, X. Castellsague, G. Ferro, P. Brennan, P. Boffetta, M. Hashibe, Sexual behaviours and the risk of head and neck cancers: a pooled analysis in the International Head and Neck Cancer Epidemiology (INHANCE) consortium, Int. J. Epidemiol. (2009), https://doi.org/10.1093/ije/dyp350.
[5] A. Santoro, G. Pannone, R. Ninivaggi, M. Petruzzi, A. Santarelli, G.M. Russo, S. Lepore, M. Pietrafesa, I. Laurenzana, R. Leonardi, P. Bucci, M.I. Natalicchio, A. Lucchese, S. Papagerakis, P. Bufo, Relationship between CK19 expression, deregulation of normal keratinocyte differentiation pattern and high risk-human papilloma virus infection in oral and oropharyngeal squamous cell carcinoma, Infect. Agents Cancer (2015), https://doi.org/10.1186/s13027-015-0041-x.
[6] C.A. Moody, L.A. Laimins, Human papillomavirus oncoproteins: pathways to transformation, Nat. Rev. Cancer (2010), https://doi.org/10.1038/nrc2886.
[7] M. Zhang, J. Liang, Y. Yang, H. Liang, H. Jia, D. Li, Current trends of targeted drug delivery for oral cancer therapy, Front. Bioeng. Biotechnol. (2020), https://doi.org/10.3389/fbioe.2020.618931.
[8] M. Poonia, K. Ramalingam, S. Goyal, S. Sidhu, Nanotechnology in oral cancer: a comprehensive review, J. Oral Maxillofac. Pathol. (2017), https://doi.org/10.4103/jomfp.JOMFP_29_17.
[9] K. Konopka, B. Fallah, J. Monzon-Duller, N. Overlid, N. Düzgünes, Serum-resistant gene transfer to oral cancer cells by Metafectene and GeneJammer: application to HSV-tk/ganciclovir-mediated cytotoxicity, Cell. Mol. Biol. Lett. (2005).
[10] S.L. Gosangari, K.L. Watkin, Effect of preparation techniques on the properties of curcumin liposomes: characterization of size, release and cytotoxicity on a squamous oral carcinoma cell line, Pharmaceut. Dev. Technol. (2012), https://doi.org/10.3109/10837450.2010.522583.
[11] K. Hariharan, T. Mehta, J. Shah, H. Dave, A. Sami, A. Omri, Localized delivery of Erlotinib using liposomal gel formulations for the treatment of oral squamous cell carcinoma, Int. J. Pharm. (2023), https://doi.org/10.1016/j.ijpharm.2023.123144.
[12] A. Mohan, S. Narayanan, G. Balasubramanian, S. Sethuraman, U.M. Krishnan, Dual drug loaded nanoliposomal chemotherapy: a promising strategy for treatment of head and neck squamous cell carcinoma, Eur. J. Pharm. Biopharm. (2016), https://doi.org/10.1016/j.ejpb.2015.11.017.
[13] E.S.A. El-Hamid, A.M. Gamal-Eldeen, A.M. Sharaf Eldeen, Liposome-coated nano doxorubicin induces apoptosis on oral squamous cell carcinoma CAL-27 cells, Arch. Oral Biol. (2019), https://doi.org/10.1016/j.archoralbio.2019.05.011.
[14] N.V. Velloso, Aluminum-phthalocyanine chloride-based photodynamic therapy inhibits PI3K/Akt/Mtorpathway in oral squamous cell carcinoma cells in vitro, Chemother. Open Access (2012), https://doi.org/10.4172/2167-7700.1000107.
[15] J. Lopes-Nunes, P.A. Oliveira, C. Cruz, G-Quadruplex-Based drug delivery systems for cancer therapy, Pharmaceuticals 14 (2021) 671, https://doi.org/10.3390/ph14070671.
[16] J. Carvalho, J.L. Mergny, G.F. Salgado, J.A. Queiroz, C. Cruz, G-Quadruplex, friend or foe: the role of the G-quartet in anticancer strategies, Trends Mol. Med. 26 (2020) 848–861, https://doi.org/10.1016/j.molmed.2020.05.002.
[17] V.R. Sharma, S.D. Thomas, D.M. Miller, F. Rezzoug, Nucleolin overexpression confers increased sensitivity to the anti-nucleolin aptamer, AS1411, Cancer Invest. 0 (2018) 1–17, https://doi.org/10.1080/07357907.2018.1527930.
[18] J. Carvalho, J. Lopes-Nunes, A.C. Lopes, M.P. Cabral Campello, A. Paulo, J. A. Queiroz, C. Cruz, Aptamer-guided acridine derivatives for cervical cancer, Org. Biomol. Chem. 17 (2019) 2992–3002, https://doi.org/10.1039/c9ob00318e.
[19] T. Santos, J. Lopes-Nunes, D. Alexandre, A. Miranda, J. Figueiredo, M.S. Silva, J. L. Mergny, C. Cruz, Stabilization of a DNA aptamer by ligand binding, Biochimie 200 (2022) 8–18, https://doi.org/10.1016/j.biochi.2022.05.002.
[20] C.M. Berger, X. Gaume, P. Bouvet, The roles of nucleolin subcellular localization in cancer, Biochimie (2015), https://doi.org/10.1016/j.biochi.2015.03.023.
[21] P.J. Bates, E.M. Reyes-Reyes, M.T. Malik, E.M. Murphy, M.G. O'Toole, J.O. Trent, G-quadruplex oligonucleotide AS1411 as a cancer-targeting agent: uses and mechanisms, Biochim. Biophys. Acta Gen. Subj. 1861 (2017) 1414–1428, https://doi.org/10.1016/j.bbagen.2016.12.015.
[22] N.Q. Do, W.J. Chung, T.H.A. Truong, B. Heddi, A.T. Phan, G-quadruplex structure of an anti-proliferative DNA sequence, Nucleic Acids Res. 45 (2017) 7487–7493, https://doi.org/10.1093/NAR/GKX274.
[23] J. Figueiredo, J. Lopes-Nunes, J. Carvalho, F. Antunes, M. Ribeiro, M.P. C. Campello, A. Paulo, A. Paiva, G.F. Salgado, J.A. Queiroz, J.-L. Mergny, C. Cruz, AS1411 derivatives as carriers of G-quadruplex ligands for cervical cancer cells, Int. J. Pharm. 568 (2019) 118511, https://doi.org/10.1016/j.ijpharm.2019.118511.
[24] J. Carvalho, J. Lopes-Nunes, M.P.C. Campello, A. Paulo, J. Milici, C. Meyers, J. L. Mergny, G.F. Salgado, J.A. Queiroz, C. Cruz, Human papillomavirus G-rich regions as potential antiviral drug targets, Nucleic Acid Therapeut. (2021), https://doi.org/10.1089/nat.2020.0869.
[25] J. Carvalho, A. Paiva, M.P. Cabral Campello, A. Paulo, J.-L. Mergny, G.F. Salgado, J.A. Queiroz, C. Cruz, Aptamer-based targeted delivery of a G-quadruplex ligand in cervical cancer cells, Sci. Rep. 9 (2019) 7945, https://doi.org/10.1038/s41598-019-44388-9.
[26] J. Carvalho, E. Pereira, J. Marquevielle, M.P.C. Campello, J.L. Mergny, A. Paulo, G. F. Salgado, J.A. Queiroz, C. Cruz, Fluorescent light-up acridine orange derivatives bind and stabilize KRAS-22RT G-quadruplex, Biochimie 144 (2018) 144–152, https://doi.org/10.1016/j.biochi.2017.11.004.
[27] E. Pereira, L. Do Quental, E. Palma, M.C. Oliveira, F. Mendes, P. Raposinho, I. Correia, J. Lavrado, S. Di Maria, A. Belchior, P. Vaz, I. Santos, A. Paulo, Evaluation of acridine orange derivatives as DNA-targeted radiopharmaceuticals for auger therapy: influence of the radionuclide and distance to DNA, Sci. Rep. 7 (2017) 1–16, https://doi.org/10.1038/srep42544.
[28] H. Nsairat, I.S. Mahmoud, F. Odeh, D. Abuarqoub, H. Al-Azzawi, R. Zaza, M. I. Qadri, S. Ismail, A. Al Bawab, A. Awidi, W. Alshaer, Grafting of anti-nucleolin aptamer into preformed and remotely loaded liposomes through aptamer-cholesterol post-insertion, RSC Adv. 10 (2020) 36219–36229, https://doi.org/10.1039/d0ra07325c.
[29] I. Maocha, B. Rosado, J. Lopes-nunes, M. Lopes, J. Rolo, B. Pires, A. Palmeira-de-oliveira, J. Martinez-de-oliveira, R.P. De Oliveira, Imiquimod-loaded nanosystem for treatment human papillomavirus-induced lesions, Pharmaceutics 16 (2024) 864, https://doi.org/10.3390/pharmaceutics16070864.
[30] W. Lin, N. Yao, H. Li, S. Hanson, W. Han, C. Wang, L. Zhang, Co-delivery of imiquimod and plasmid DNA via an amphiphilic pH-responsive star polymer that forms unimolecular micelles in water, Polymers (2016), https://doi.org/10.3390/polym8110397.
[31] J. Carvalho, J. Lopes-Nunes, B. Vialet, T. Rosado, E. Gallardo, J. Vale, C. Eloy, S. Ferreira, R. Palmeira-de-Oliveira, M.P.C. Campello, A. Paulo, P. Barthélémy, J. L. Mergny, G.F. Salgado, J.A. Queiroz, A.D. Ellington, C. Cruz, Nanoaggregate-forming lipid-conjugated AS1411 aptamer as a promising tumor-targeted delivery system of anticancer agents in vitro, Nanomed. Nanotechnol. Biol. Med. (2021), https://doi.org/10.1016/j.nano.2021.102429.
[32] J. Lopes-Nunes, A.S. Agonia, T. Rosado, E. Gallardo, R. Palmeira-De-oliveira, A. Palmeira-De-oliveira, J. Martinez-De-oliveira, J. Fonseca-Moutinho, M.P. C. Campello, A. Paiva, A. Paulo, A. Vulgamott, A.D. Ellignton, P.A. Oliveira, C. Cruz, Aptamer-functionalized gold nanoparticles for drug delivery to gynecological carcinoma cells, Cancers (2021), https://doi.org/10.3390/cancers13164038.
[33] E. Wolfson, S. Solomon, E. Schmukler, Y. Goldshmit, R. Pinkas-Kramarski, Nucleolin and ErbB2 inhibition reduces tumorigenicity of ErbB2-positive breast cancer article, Cell Death Dis. (2018), https://doi.org/10.1038/s41419-017-0067-7.
[34] C.C. Liang, A.Y. Park, J.L. Guan, In vitro scratch assay: a convenient and inexpensive method for analysis of cell migration in vitro, Nat. Protoc. (2007), https://doi.org/10.1038/nprot.2007.30.
[35] J. Yu, X. Xie, L. Wang, W. Liu, H. Xu, X. Lu, X. Li, J. Ren, W. Li, Smart chondroitin sulfate micelles for effective targeted delivery of doxorubicin against breast cancer metastasis, Int. J. Nanomed. (2023), https://doi.org/10.2147/IJN.S398802.
[36] İ. Eroğlu, E. Azizoğlu, M. Özyazıcı, M. Nenni, H. Gürer Orhan, S. Özbal, I. Tekmen, İ. Ertam, İ. Ünal, Ö. Özer, Effective topical delivery systems for corticosteroids: dermatological and histological evaluations, Drug Deliv. (2016), https://doi.org/10.3109/10717544.2014.960981.
[37] D. Guimarães, A. Cavaco-Paulo, E. Nogueira, Design of liposomes as drug delivery system for therapeutic applications, Int. J. Pharm. (2021), https://doi.org/10.1016/j.ijpharm.2021.120571.
[38] A. Gouda, O.S. Sakr, M. Nasr, O. Sammour, Ethanol injection technique for liposomes formulation: an insight into development, influencing factors, challenges and applications, J. Drug Deliv. Sci. Technol. (2021), https://doi.org/10.1016/j.jddst.2020.102174.
[39] Z. Cao, R. Tong, A. Mishra, W. Xu, G.C.L. Wong, J. Cheng, Y. Lu, Reversible cell-specific drug delivery with aptamer-functionalized liposomes, Angew. Chem. Int. Ed. 48 (2009) 6494–6498, https://doi.org/10.1002/anie.200901452.
[40] Z.X. Liao, E.Y. Chuang, C.C. Lin, Y.C. Ho, K.J. Lin, P.Y. Cheng, K.J. Chen, H.J. Wei, H.W. Sung, An AS1411 aptamer-conjugated liposomal system containing a bubble-generating agent for tumor-specific chemotherapy that overcomes multidrug resistance, J. Contr. Release 208 (2015) 42–51, https://doi.org/10.1016/j.jconrel.2015.01.032.
[41] H. Xinga, L. Tang, X. Yang, K. Hwang, W. Wang, Q. Yin, N.Y. Wong, L.W. Dobrucki, N. Yasui, J.A. Katzenellenbogen, W.G. Helferich, J. Cheng, Y. Lu, Selective delivery of an anticancer drug with aptamer- functionalized liposomes to breast cancer cells in vitro and in vivo, J. Mater. Chem. B 1 (2013) 5288–5297, https://doi.org/10.1039/C3TB20412J.

[42] E.M. Reyes-Reyes, Y. Teng, P.J. Bates, A new paradigm for aptamer therapeutic AS1411 action: uptake by macropinocytosis and its stimulation by a nucleolin-dependent mechanism, Cancer Res. 70 (2010) 8617–8629, https://doi.org/10.1158/0008-5472.CAN-10-0920.

[43] M.T. Malik, M.G. O'Toole, L.K. Casson, S.D. Thomas, G.T. Bardi, E.M. Reyes-Reyes, C.K. Ng, K.A. Kang, P.J. Bates, AS1411-conjugated gold nanospheres and their potential for breast cancer therapy, Oncotarget 6 (2015) 22270–22281, https://doi.org/10.18632/oncotarget.4207.

[44] C. Riccardi, C. Fàbrega, S. Grijalvo, G. Vitiello, G. D'Errico, R. Eritja, D. Montesarchio, AS1411-decorated niosomes as effective nanocarriers for Ru(III)-based drugs in anticancer strategies, J. Mater. Chem. B 6 (2018) 5368–5384, https://doi.org/10.1039/c8tb01563e.

[45] I. Ugrinova, M. Petrova, M. Chalabi-Dchar, P. Bouvet, Multifaceted nucleolin protein and its molecular partners in oncogenesis, in: Adv. Protein Chem. Struct. Biol., first ed., Elsevier Inc., 2018, pp. 133–164, https://doi.org/10.1016/bs.apcsb.2017.08.001.

[46] C.S. Lee, T.W. Kim, D.E. Oh, S.O. Bae, J. Ryu, H. Kong, H. Jeon, H.K. Seo, S. Jeon, T.H. Kim, In vivo and in vitro anticancer activity of doxorubicin-loaded DNA-auNP nanocarrier for the ovarian cancer treatment, Cancers (2020), https://doi.org/10.3390/cancers12030634.

[47] N.M. de Vasconcelos, N. Van Opdenbosch, H. Van Gorp, R. Martín-Pérez, A. Zecchin, P. Vandenabeele, M. Lamkanfi, An apoptotic caspase Network safeguards cell death induction in pyroptotic macrophages, Cell Rep. (2020), https://doi.org/10.1016/j.celrep.2020.107959.

[48] J. Noguti, C.F.G. De Moura, G.P.P. De Jesus, V.H.P. Da Silva, T.A. Hossaka, C.T. F. Oshima, D.A. Ribeiro, Metastasis from oral cancer: an overview, Cancer Genomics Proteomics (2012).

[49] E. Pachmayr, C. Treese, U. Stein, Underlying mechanisms for distant metastasis - molecular biology, Visc. Med. (2017), https://doi.org/10.1159/000454696.

[50] J. shun Wu, J. Jiang, B. jun Chen, K. Wang, Y. ling Tang, X. hua Liang, Plasticity of cancer cell invasion: patterns and mechanisms, Transl. Oncol (2021), https://doi.org/10.1016/j.tranon.2020.100899.

[51] W.G. Jiang, A.J. Sanders, M. Katoh, H. Ungefroren, F. Gieseler, M. Prince, S. K. Thompson, M. Zollo, D. Spano, P. Dhawan, D. Sliva, P.R. Subbarayan, M. Sarkar, K. Honoki, H. Fujii, A.G. Georgakilas, A. Amedei, E. Niccolai, A. Amin, S.S. Ashraf, L. Ye, W.G. Helferich, X. Yang, C.S. Boosani, G. Guha, M.R. Ciriolo, K. Aquilano, S. Chen, A.S. Azmi, W.N. Keith, A. Bilsland, D. Bhakta, D. Halicka, S. Nowsheen, F. Pantano, D. Santini, Tissue invasion and metastasis: molecular, biological and clinical perspectives, Semin. Cancer Biol. (2015), https://doi.org/10.1016/j.semcancer.2015.03.008.

[52] M. Wegge, R. Dok, L.J. Dubois, S. Nuyts, Use of 3D spheroid models for the assessment of RT response in head and neck cancer, Int. J. Mol. Sci. (2023), https://doi.org/10.3390/ijms24043763.

[53] V.F. Mestre, B. Medeiros-Fonseca, D. Estêvão, F. Casaca, S. Silva, A. Félix, F. Silva, B. Colaço, F. Seixas, M.M.S.M. Bastos, C. Lopes, R. Medeiros, P.A. Oliveira, R.M. Gil da Costa, HPV16 is sufficient to induce squamous cell carcinoma specifically in the tongue base in transgenic mice, J. Pathol. (n.d.). https://doi.org/10.1002/path.5387.

[54] N.M. La-Beck, A.A. Gabizon, Nanoparticle interactions with the immune system: clinical implications for liposome-based cancer chemotherapy, Front. Immunol. (2017), https://doi.org/10.3389/fimmu.2017.00416.

[55] N.M. La-Beck, X. Liu, L.M. Wood, Harnessing liposome interactions with the immune system for the next breakthrough in cancer drug delivery, Front. Pharmacol. (2019), https://doi.org/10.3389/fphar.2019.00220.

[56] Y. Liu, H. Guo, R. Xu, W. Chen, Smart intraoral systems for advanced drug delivery, MedComm - biomater, Appl. (2022), https://doi.org/10.1002/mba2.19.